frontiers in Materials

ORIGINAL RESEARCH
published: 09 January 2018
doi: 10.3389/fmats.2017.00047

Si@SiO$_x$/Graphene Nanosheets Composite: Ball Milling Synthesis and Enhanced Lithium Storage Performance

Xiaoyong Tie[1], Qianyan Han[2], Chunyan Liang[1], Bo Li[2], Jiantao Zai[2] and Xuefeng Qian[2]*

[1] Hubei Land Resources Vocational College, Wuhan, China, [2] Shanghai Electrochemical Energy Devices Research Center, School of Chemistry and Chemical Engineering, State Key Laboratory of Metal Matrix Composites, Shanghai Jiao Tong University, Shanghai, China

Si@SiO$_x$/grapheme nanosheet (Si@SiO$_x$/GNS) nanocomposites as high-performance anode materials for lithium-ion batteries are prepared by mechanically blending the mixture of expanded graphite (EG) with Si nanoparticles, and characterized by Raman spectrum, X-ray diffraction (XRD), field emission scanning electron microscopy, and transmission electron microscopy. During ball milling process, the size of Si nanoparticles will decrease, and the layer of EG can be peeled off to thin multilayers. Electrochemical tests reveal that the Si@SiO$_x$/GNS nanocomposites show enhanced cycling stability, high reversible capacity, and rate capability, even with high content of active materials of 80% and without electrolyte additives. The retained revisable capacity is 1,055 mAh g^{-1} after 50 cycles at 0.2 A g^{-1} and about 63.6% of the initial value. The great electrochemical performance of Si@SiO$_x$/GNS nanocomposites can be ascribed to GNS prepared through heat-treat and ball-milling methods, the decrease in the size of Si nanoparticles and SiO$_x$ layer on Si surface, which enhance the interactions between Si and GNS.

Keywords: silicon, silicon oxide, GNS, ball milling, lithium ion batteries

OPEN ACCESS

Edited by:
Xiaoxin Zou,
Jilin University, China

Reviewed by:
Fang Dai,
General Motors, United States
Ran Yi,
Pacific Northwest National Laboratory (DOE), United States

****Correspondence:***
Xiaoyong Tie
xiaoyongtie@163.com

Specialty section:
This article was submitted to Colloidal Materials and Interfaces, a section of the journal Frontiers in Materials

Received: *21 August 2017*
Accepted: *11 December 2017*
Published: *09 January 2018*

Citation:
Tie X, Han Q, Liang C, Li B, Zai J and Qian X (2018) Si@SiO$_x$/Graphene Nanosheets Composite: Ball Milling Synthesis and Enhanced Lithium Storage Performance. Front. Mater. 4:47. doi: 10.3389/fmats.2017.00047

INTRODUCTION

Lithium-ion batteries have been widely used in consumer electronics, electrical vehicles, and energy storage market (Tarascon and Armand, 2001; Chan et al., 2008; Li et al., 2009; Huang et al., 2013; Rahman et al., 2016). In recent years, lots of efforts have been put in exploring anode materials with higher specific capacities over graphite. Silicon-based materials have attracted considerable research attentions as one of the most promising anode materials for lithium-ion batteries because of its highest theoretical capacity (4,200 mAh g^{-1}) during the formation of $Li_{4.4}Si$ alloys (Netz and Huggins, 2004; Chan et al., 2008; Teki et al., 2009; Winter et al., 2010; Ji et al., 2011; Yue et al., 2013; Wang et al., 2015). However, the huge volume changes during lithiation and de-lithiation process always leads to poor cycle performance and electrical contact, which severely hinders the industrial applications of silicon-based anode materials (Candace et al., 2009; Hertzberg et al., 2010; Bo et al., 2016; Li et al., 2016, 2017). Currently, some approaches have been designed to accommodate the volume change by introducing void spaces or improving the linkage between Si particles, and further enhance the cycling performance of Si materials, such as decreasing Si into nanoscale size (Chen et al., 2010; Szczech and Jin, 2010; Hu et al., 2011; Liu et al., 2011, 2015) (e.g., silicon nanowires,

silicon nanotubes, and silicon nanoarrays); developing Si into thin-film electrodes (Arie et al., 2009; Tao et al., 2011); optimizing the morphology of silicon to improve the electronic contact of silicon with current collector (Zheng et al., 2007; Peng et al., 2010) or dispersing silicon into a dimensional stable matrix (Ng et al., 2006; Zhang et al., 2010; Yi et al., 2013). On the other hand, SiO_x nanocomposites also have attracted considerable attention because the *in situ* generated Li_2O during the first discharge process can buffer the volume changes during lithiation/delithiation process and further improve the cycling performance of electrode (Hu et al., 2008). For example, core double-shell Si@SiO_2@C nanocomposites were produced through hydrothermal and annealing process, and displayed stable cycling performance even in the VC-free electrolyte (Liwei et al., 2010). Furthermore, some groups also successfully prepared SiO_x anodes with great cycle performances (Guo et al., 2012; Xin et al., 2012).

Recently, GNS has been attracted great attention because of its intriguing properties in good electrical conductivity, high surface area, unique heterogeneous, etc. (Bunch et al., 2007; Dikin et al., 2007; Geim and Novoselov, 2007), and several routes have been established to prepare GNS, such as chemical reduction of exfoliated graphite oxide, chemical vapor deposition, thermal reduction of graphite oxide, and others. However, these methods do not fit at the moment for manufacturing electrodes because of tedious and expensive mass production. Two economic ways have been explored to prepare GNS on large scale. One is exfoliation of graphite using ball milling, and another way is to treat the expandable graphite with high temperature (Zhao et al., 2010a; León et al., 2011; Xiang et al., 2011; Yan et al., 2012). In present work, Si@SiO$_x$/GNS nanocomposites have been produced by a simple ball milling method, and the result Si@SiO$_x$/GNS nanocomposites exhibit good cycling stability, high reversible capacity, and rate capability as anode materials for Lithium-ion batteries.

EXPERIMENTAL

Synthesis of Si@SiO*x*/GNS Nanocomposites

Expandable graphite was supplied by Qingdao Haida Co., Ltd. Si nanoparticles with average particle size of ~120 nm were bought from Hefei Kaier Nanotechnology Co., Ltd. In a typical process, expanded graphite (EG) was firstly prepared by expanding expandable graphite through rapid thermal expansion at 600°C for 10 min. Then, a mixture of Si nanoparticles and the as-prepared EG was milled at the speed of 500 rpm for 15 h in a planetary machine (QM-3SP04) with 30 agate balls in the diameter of 0.8 mm, and then, Si@SiO$_x$/GNS nanocomposites were obtained (**Scheme 1**). The obtained Si@SiO$_x$/GNS nanocomposites were labeled as SG1, SG2, and SG3, respectively, with weight ratios of Si nanoparticles to EG as 1:1, 1:2, 2:1. In the similar way, Si@SiO$_x$/expandable graphite was also obtained and denoted as SEG for comparison.

Characterization

Morphology of the samples was characterized by scanning electron microscopy (SEM) (JSM-7401F) and TEM (JEOL, JEM-2100). X-ray diffraction (XRD) was recorded with Cu-Ka radiation, and the current and voltage of X-ray tube is of 30 mA and 40 kV, respectively. Raman spectrum was recorded with a holographic grating of 1,800 g/mm. X-ray photoelectron spectroscopy (XPS) analysis was performed to confirm the oxidation state of obtained products. Fourier-transform infrared spectrum was conducted on a Perkin 1000 instrument over 4,000–450 cm^{-1}. Thermogravimetric analysis (TGA) was carried out to determine the weight ratio of GNS in Si@SiO$_x$/GNS.

Electrochemical Measurement

Electrodes were made of Si@SiO$_x$/GNS nanocomposite, acetylene black, and polyvinylidene difluoride in weight ratio of 80:10:10. Afterward, the slurry was spread onto a Cu current collector foil, then dried at 70°C for 6 h in vacuum. The typical mass loading of Si@SiO$_x$/GNS nanocomposite on the electrode was about 1.0 mg/cm^2. Then, 2016-type Coin cells were assembled using polypropylene membrane as separator in an argon-filled glove box with concentration of oxygen and moisture below 1.0 ppm. Electrolyte was 1 mol/L of $LiClO_4$ in a mixture of ethylene carbonate/diethylene carbonate (50:50 vol%). Coin cells were assembled with the as-prepared Si@SiO$_x$/GNS electrode as anode and Li as counter electrode. Cycling of cells was tested between 0.01 and 3 V vs Li^+/Li using LAND CT2001A model battery test instrument.

RESULTS AND DISCUSSION

The formation of Si@SiO$_x$/GNS nanocomposites is depicted in **Scheme 1**. A mixture of Si nanoparticles and EG is milled in a planetary machine with agate balls. During the ball milling process, the size of Si nanoparticles will decrease, and Si nanoparticles are homogeneously dispersed among nanosheets. What's more, the layers of EG would be peeled off owing to the mechanical shear stress of the agate balls and Si nanoparticles, just like the paper feeding process of a roll-fed printer (Zhao et al., 2010a;

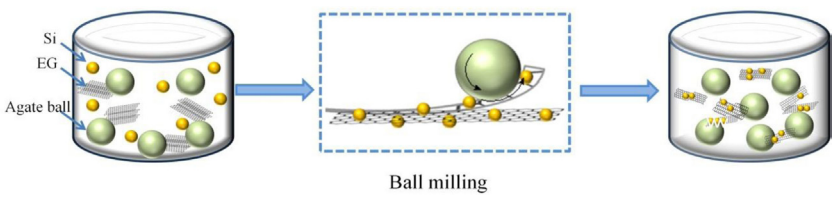

SCHEME 1 | Illustration of the synthesis process of Si@SiO$_x$/GNS nanocomposites.

León et al., 2011; Xiang et al., 2011; Yan et al., 2012). Thus, the EG will convert to graphene nanosheet and coat on Si nanoparticles.

Figure 1 shows the morphology of Si nanoparticles, EG, and Si@SiO$_x$/GNS nanocomposite (SG1). Compared the SEM images of EG (**Figure 1B**) with SG1 (**Figure 1C**), one can see that the layer of EG with about 400 nm in thickness are peeled off to thin multilayers during ball milling process. Furthermore, owing to mechanical mixing, homogeneous nanocomposites can be obtained. TEM images (**Figure 1D**) indicates that Si nanoparticles are of 50–100 nm in diameter with elliptical-shape after ball milling is smaller than that of pure Si nanoparticles without ball-milling (**Figure 1A**), indicating that ball milling process also has a great effect on the particulate size of nanocomposites.

X-ray diffraction patterns of the obtained nanocomposites (**Figure 2A**) shows that all the major peaks can be assigned to cubic silicon (JCPDS No. 89–2955). The diffraction peaks at $2\theta = 28.5°$, 47.4°, 56.2°, and 76.5°can be indexed to the diffraction peaks of silicon. The broad peak at approximately 25.5° is attributed to that of GNS. No peaks of *SiC* phases are found, implying the obtained nanocomposites are free of *SiC* during the ball milling process. Raman spectroscopy is further used to confirm the obtained Si@SiO$_x$/GNS nanocomposites (**Figure 2B**). Both the Raman spectra of pristine expandable graphite and EG display a clear 2D-band located at the frequency of 2,727 cm^{-1}, which is consistent with the multi-layer feature of bulk graphite. Comparing the Raman spectra of pristine expandable graphite with EG, heat-treatment process does not change the structure of expandable graphite. However, the intensity of 2D-peak decreases and appreciable D-peak signal can be observed after ball milling process, implying the significant disorder of expandable graphite and/or EG in the obtained nanocomposites. In addition, the ratio of the intensity of D and G peaks (I_D/I_G) for the as-prepared samples remarkably increases, indicating a reduced degree of graphitization (Luo et al., 2016a,b). The results are matching well with the previously reported data for GNS (Tang et al., 2009; Zhao et al., 2010b), implying the successful conversion of EG to GNS. In the Raman spectra of SEG and SG1, the sharp peak of 516 cm^{-1} corresponds to crystalline silicon, and the intensity of SG1 is higher than that of SEG, implying that both the heat and milling treatment of expandable graphite help to decrease the size of Si particles. From **Figure 2C**, one can clearly find the Si2p, O1s, and C1s typical peaks in the XPS spectra of SG1, indicating that the as-prepared samples consists of C and O. The O1s peak can be mainly ascribed to C-O, C = O, and Si-O types of O atom. The peak at 99.5 eV can be assigned to crystalline Si, and the peak at 103 eV in the high resolution is indicative of the presence of SiO$_x$ ($x < 2$) (Kim et al., 2010; Yang et al., 2017), which is mainly derived from the oxidation of Si particles during ball milling process. FT-IR is further carried out to study the effect of SiO$_x$ in the final products (**Figure 2D**). In the case of EG, peaks centered at 3,458 and 1,639 cm^{-1} can be indexed to the adsorbed water. The peaks at around 1,367, 1,108, and 620 cm^{-1} are indexed to methylene group, P-O bond and Cl-O bond, respectively. For the spectra of SG1 and Si, the peaks at about 1,100, 800, and 450 cm^{-1} are assigned to Si-O bond. Before ball milling process, a pretreatment for Si nanoparticles using 20% HF are applied. Therefore, the SiO$_x$ in pristine Si nanoparticles are probably derived by surface oxidation of Si nanoparticles in sample preparation of FT-IR. The peak intensities of Si-O bond for SG1 are stronger than that for pure Si nanoparticles, which indicates that the mixtures are further oxidized by ball milling. Through the FT-IR spectra of the three samples, we can also find that the peak intensities of Si-O bond and methylene group for SG1 are different from that of other samples, implying some chemical interactions between SiO$_x$ and the groups of GNS surface. The amount of Si@SiO$_x$ in the Si@SiO$_x$/GNS nanocomposites is about 58 wt% if we suppose GNS reacting with O_2 in air to produce CO_2 and the final resultants only including Si and SiO$_x$ (**Figure 3**).

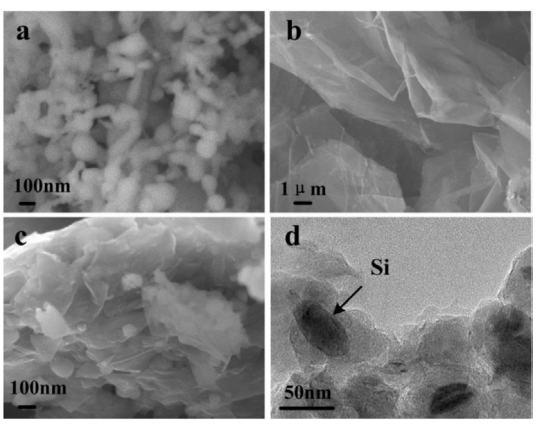

FIGURE 1 | FESEM images of Si nanoparticles **(A)**, expanded graphite **(B)**, Si@SiO$_x$/GNS nanocomposite (SG1) **(C)**, and TEM image of SG1 **(D)**.

Electrochemical performances of the as-obtained SG1 and SEG are displayed in **Figure 4**. From the charge/discharge curves at the 1st, 2nd, 10th, 20th, and 40th cycle of SG1 and SEG under a current density of 200 mA g^{-1} (**Figures 4A,B**), it can be found that SG1 and SEG show discharge capacities of 1,658.3 and 1,663.7 mAh g^{-1} at the first cycle, corresponding the Coulombic efficiencies of about 67.2 and 69.3%, respectively. At the second cycle, the discharge capacity of SG1 and SEG decreases to 1,498.9 and 1,207 mAh g^{-1}, respectively, maintaining 90.4 and 72.5% to the initial value. The irreversible capacity loss of these nanocomposites can be ascribed to the formation of a solid electrolyte interphase film on GNS surface, which consumes plenty of Li ions (Wang et al., 2009). One can also note that both the composites show increasing capacity in first cycles because of the activation process coming from the reconstruction of crystal structure of Si, in which the Li–Si alloying/dealloying process leads to in significant internal structural changes of Si anode (Shin et al., 2005; Guo et al., 2010; Xin et al., 2012; Luo et al., 2016a,b), and then, the Li^+ diffusion and electrochemical kinetics reach an optimal state after several cycles.

Figure 5A shows the cycling performances of SG1, SEG, and pure Si materials. Te capacity of pure Si electrode drops dramatically to ~300 mAh g^{-1} after 20 cycles, showing the poor cycling stability. One can also see that both SG1 and SEG electrodes shows higher initial reversible capacity of pure Si electrode of only 965.7 mAh g^{-1}, which is because of the smaller size of Si nanoparticles after ball milling and better dispersion of nanosized

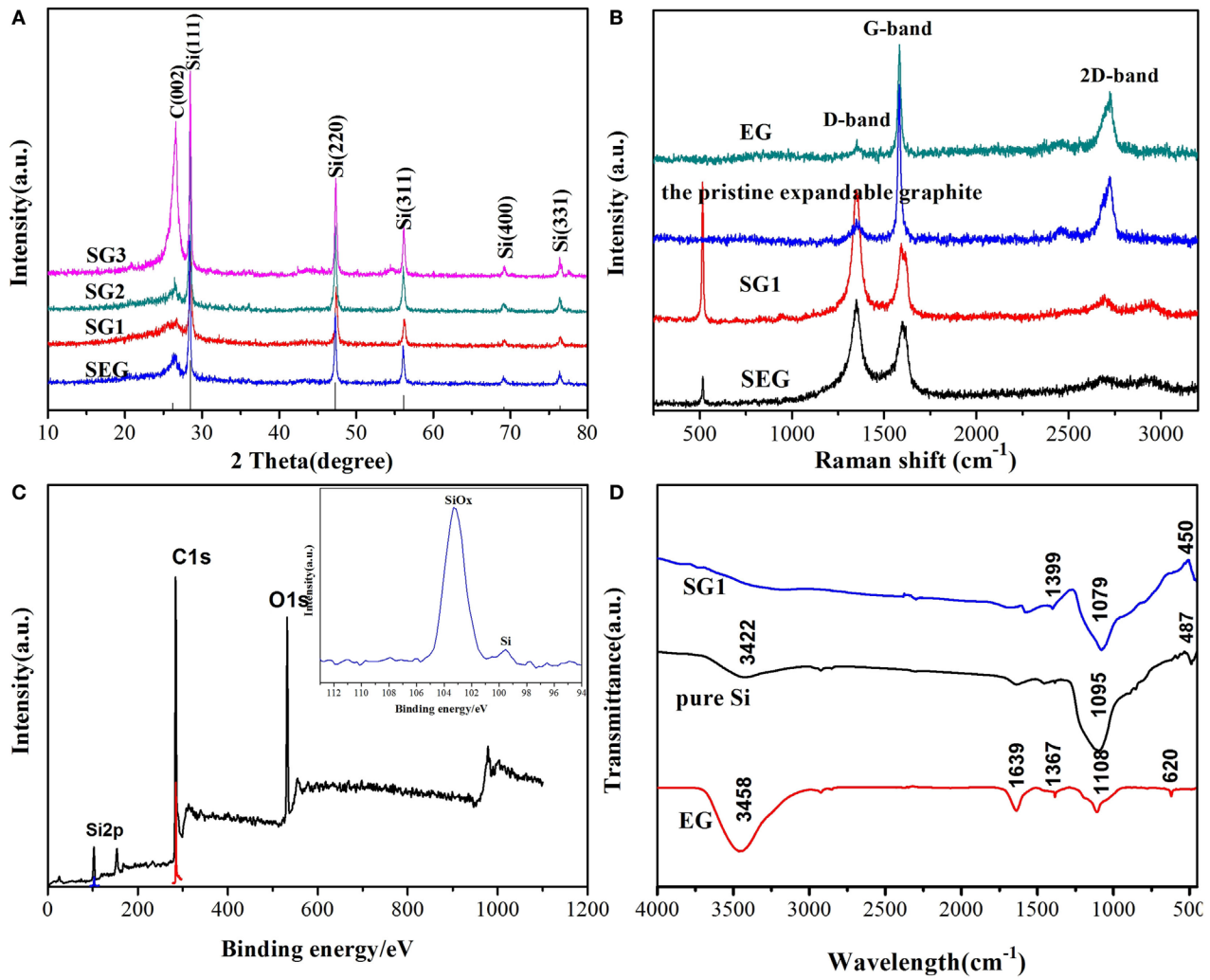

FIGURE 2 | X-ray diffraction spectra of SG1, SG2, SG3, and Si@SiO$_x$/expandable graphite (SEG) **(A)**, Raman spectra of pristine expandable graphite, expanded graphite (EG), SG1, and SEG **(B)**, X-ray photoelectron spectroscopy spectra of SG1 with the high-resolution spectrum of Si 2p (inserted) **(C)**, FT-IR spectra of EG, Si nanoparticles, and SG1 **(D)**.

Si in the as-prepared composites could be helpful to enhance the electrochemical performance of electrodes. Furthermore, the cycling abilities are obviously improved when Si nanoparticles are complexed with GNS or graphite, and SG1 reveals a better cyclic ability than that of SEG. Although the initial capacity of SG1 electrode is slightly lower than SEG anode, the reversible capacity is retained as 1,055 mAh g^{-1} after 50 cycles, which is 63.6% of the initial value, while SEG presents a fast capacity fading. The dramatic difference performances of SG1 and SEG may due to the heat-treat process, which can enlarge the void space between nanosheets and offer more free space for the volume change of Si.

For comparison, the electrochemical evaluations of SG2 and SG3 are also carried out (**Figure 6**), and SG1 electrode shows the greatest enhancement of the capacity retention. Because the SG 2 and SG3 have different composition ratios between Si and EG, the ball milling behaviors may not be equal to the SG1, which may affect the capacity and cycle performances of SG1, SG2, and SG3. The bad cycling performance of SG2 and SG3 can be resulted to less weight ratio of Si nanoparticles or more serious volume effect, respectively. The rate performance of SG1 is shown in **Figure 5B**, the specific capacity at 0.2, 0.5, 1, and 2 A g^{-1} are 1,121, 967, 718, and 470 mAh g^{-1}, respectively, demonstrating its better rate performance. Noticeably, a stable high reversible capacity of 1,196 mAh g^{-1} is still reserved when the current density returns to 0.2 A g^{-1} at the 41th cycle.

In general, the electrochemical improvement of electrode ascribes to the following reasons (as shown in **Scheme 2B**). First, the decrease in the size of Si nanoparticles with ball milling process and the homogeneously dispersion among GNS could impede the aggregation of Si nanoparticles. Besides the enhanced conductivity by GNS, the as-prepared Si@SiO$_x$/GNS nanocomposites show higher specific initial capacity than pure Si materials. Second, as illuminated in **Scheme 2A**, the void between GNS can offer many free space to accommodate the huge

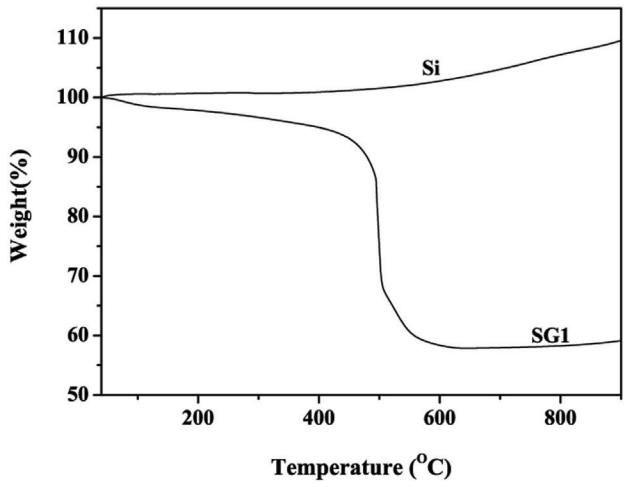

FIGURE 3 | Thermogravimetric analysis curves of Si nanoparticles and SG1.

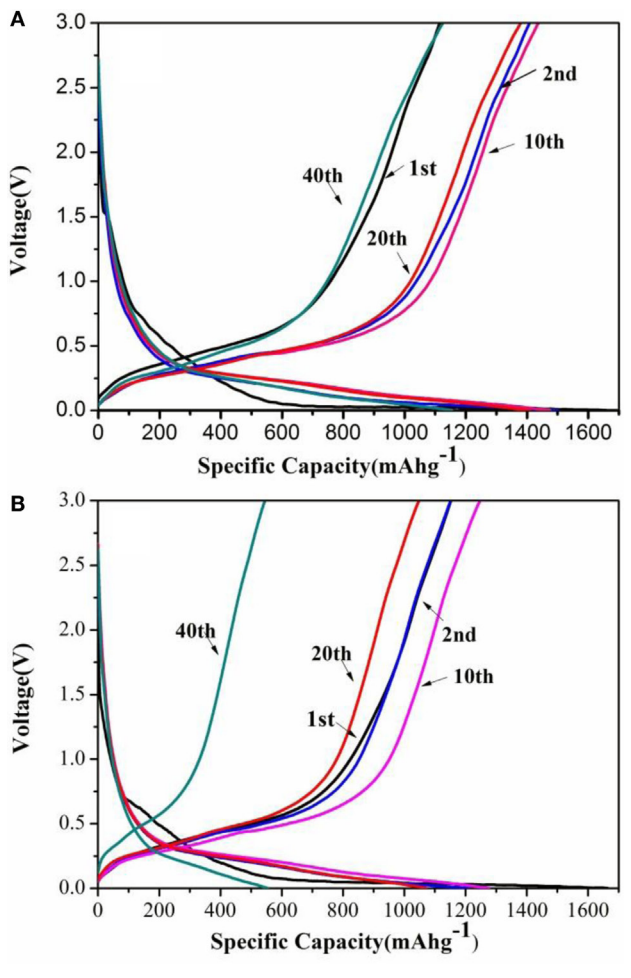

FIGURE 4 | Typical charge–discharge curves of SG1 **(A)** and SEG **(B)** cycled at the 1st, 2nd, 10th, 20th, and 40th between 0.01 and 3.0 V.

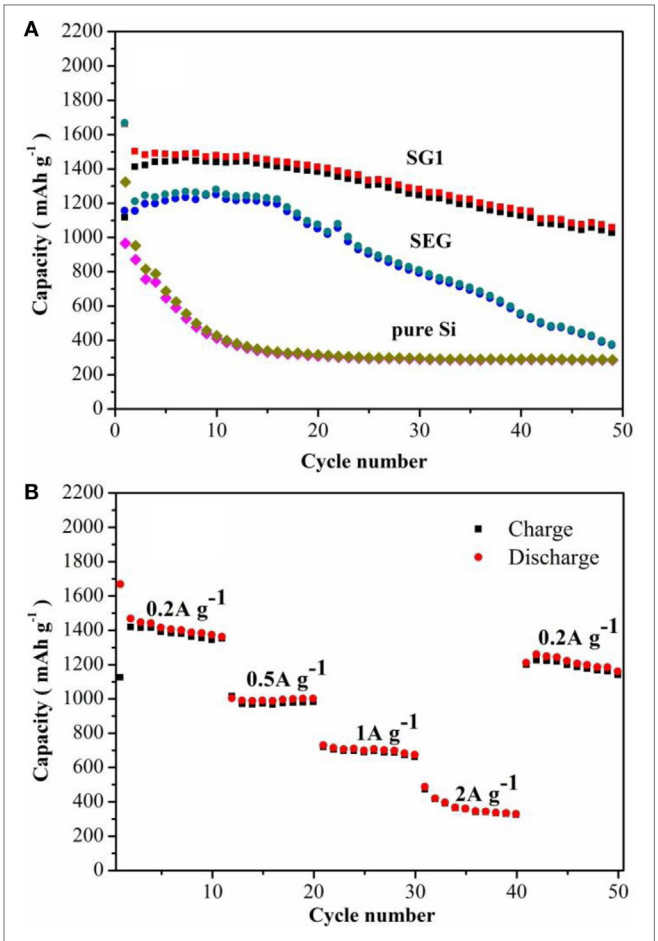

FIGURE 5 | **(A)** Cycling performance of pure Si, SG1, and SEG, **(B)** rate performance of SG1 at current densities from 0.2 to 2.0 A g^{-1} between 0.01 and 3.0 V.

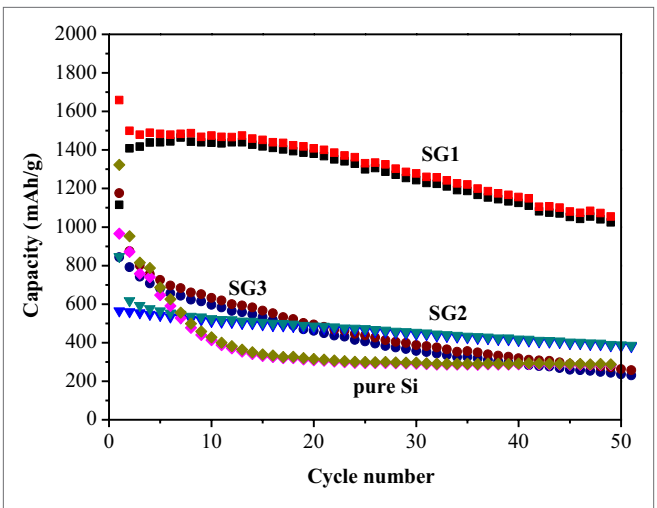

FIGURE 6 | Cycling performance of Si, SG1, SG2, and SG3 anodes at 0.2 A g^{-1}.

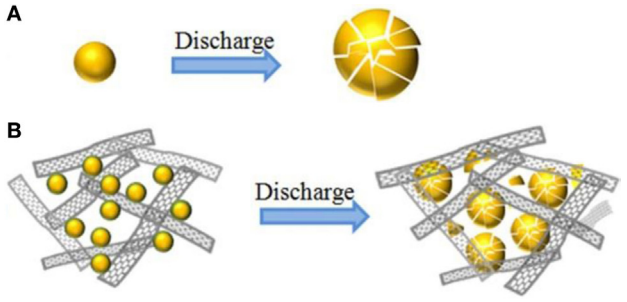

SCHEME 2 | Schematic illustration of structure evolution of pure Si material **(A)** and Si@SiO$_x$/GNS composite **(B)** during lithiation.

volume variation of Si during cycling, and maintain the integrity of electrode. At the same time, the void space between GNS could favor the diffusion of Li^+ and electrons and facilitate the accessibility of electrolyte. Finally, though SiO_x reduces the reversible capacity and Coulombic efficiency of Si anode, the SiO_x layer may improve the adhesion of Si and GNS, so, the cycling stability of Si anode is effectively enhanced (Liwei et al., 2010; Xin et al., 2012). Meanwhile, the generated Li_2O can also buffer volume changes. Thus, the obtained composite show enhanced cycling stability, high reversible capacity and rate capability, even with high content of active materials of 80% and without electrolyte additives.

CONCLUSION

Si@SiO$_x$/GNS nanocomposites are successfully prepared through a simple ball-milling method. The as-prepared material shows enhanced cycling stability, high reversible capacity, and rate capability, even with high content of active materials of 80% and without electrolyte additives. The reversible capacity is retained ~1,055 mAh g^{-1} after 50 cycles at 0.2 A g^{-1}. The enhanced performance of Si@SiO$_x$/GNS composite can be ascribed to the reduced size of Si nanoparticles, SiO_x layer and synergistic effect of GNS. Although the Coulombic efficiency and rate performance could be further improved, Si@SiO$_x$/GNS nanocomposites show great promising as anode materials for lithium-ion batteries for the simple fabrication process, capability to traditional electrolyte system and high content of active materials.

AUTHOR CONTRIBUTIONS

JZ and XT proposed the work, did the fabrication of materials, and wrote the manuscript. QH, CL, and BL performed the material characterization and LIB testing, performed the synthesis of materials.

FUNDING

This work are supported by the Research project of Hubei Geological Bureau (KJ2017-27), the Program of National Natural Science Foundation of China (21501120 and 21331004), Research project of environmental protection in Jiangsu province (2016060), National Basic Research Program of China (2014CB239702), Science and Technology Commission of Shanghai Municipality (14DZ2250800), Plan for Scientific Innovation Talent of Henan Province (174200510017).

REFERENCES

Arie, A. A., Chang, W., and Lee, J. K. (2009). Effect of fullerene coating on silicon thin film anodes for lithium rechargeable batteries. *J. Sol. St. Electrochem.* 14, 51–56. doi:10.1007/s10008-009-0787-4

Bo, L., Xiaomin, L., Jiantao, Z., and Xuefeng, Q. (2016). Facile synthesis of porous Zn-Sn-O nanocubes and their electrochemical performances. *Nano Micro Lett.* 8, 174–181. doi:10.1007/s40820-015-0075-z

Bunch, J. S., Zande, A. M. V. D., Verbridge, S. S., Frank, I. W., Tanenbaum, D. M., Parpia, J. M., et al. (2007). Electromechanical resonators from graphene sheets. *Science* 315, 490–493. doi:10.1126/science.1136836

Candace, K. C., Riccardo, R., Seung Sae, H., Robert, A. H., and Yi, C. (2009). Structural and electrochemical study of the reaction of lithium with silicon nanowires. *J. Power Sources* 189, 34–39. doi:10.1016/j.jpowsour.2008.12.047

Chan, C. K., Peng, H., Liu, G., McIlwrath, K., Zhang, X. F., Huggins, R. A., et al. (2008). High-performance lithium battery anodes using silicon nanowires. *Nat. Nanotechnol.* 3, 187–191. doi:10.1038/nnano.2007.411

Chen, X., Gerasopoulos, K., Guo, J., Brown, A., Wang, C., Ghodssi, R., et al. (2010). Virus-enabled silicon anode for lithium-ion batteries. *ACS Nano* 4, 5366–5372. doi:10.1021/nn100963j

Dikin, D. A., Stankovich, S., Zimney, E. J., Piner, R. D., Dommett, G. H., Evmenenko, G., et al. (2007). Preparation and characterization of graphene oxide paper. *Nature* 448, 457. doi:10.1038/nature06016

Geim, A. K., and Novoselov, K. S. (2007). The rise of graphene. *Nat. Mater.* 6, 183–191. doi:10.1038/nmat1849

Guo, H., Mao, R., Yang, X., and Chen, J. (2012). Hollow nanotubular SiO_x templated by cellulose fibers for lithium ion batteries. *Electrochim. Acta* 74, 271–274. doi:10.1016/j.electacta.2012.04.086

Guo, J., Sun, A., and Wang, C. (2010). A porous silicon-carbon anode with high overall capacity on carbon fiber current collector. *Electrochem. commun.* 12, 981–984. doi:10.1016/j.elecom.2010.05.006

Hertzberg, B., Alexeev, A., and Yushin, G. (2010). Deformations in Si-Li anodes upon electrochemical alloying in nano-confined space. *J. Am. Chem. Soc.* 132, 8548–8549. doi:10.1021/ja1031997

Hu, L., Wu, H., Hong, S. S., Cui, L., McDonough, J. R., Bohy, S., et al. (2011). Si nanoparticle-decorated Si nanowire networks for Li-ion battery anodes. *Chem. Commun.* 47, 367–369. doi:10.1039/c0cc02078h

Hu, Y. S., Demir-Cakan, R., Titirici, M. M., Muller, J. O., Robert, S., Markus, A., et al. (2008). Superior storage performance of a Si@SiO$_x$/C nanocomposite as anode material for lithium-ion batteries. *Angew. Chem. Int. Ed. Engl.* 47, 1645. doi:10.1002/anie.200704287

Huang, S., Guo, H., Li, X., Wang, Z., Gan, L., Wang, J., et al. (2013). Carbonization and graphitization of pitch applied for anode materials of high power lithium ion batteries. *J. Sol. St. Electrochem.* 17, 1401–1408. doi:10.1007/s10008-013-2003-9

Ji, L., Lin, Z., Alcoutlabi, M., and Zhang, X. (2011). Recent developments in nanostructured anode materials for rechargeable lithium-ion batteries. *Energy Environ. Sci.* 4, 2682–2699. doi:10.1039/c0ee00699h

Kim, H., Seo, M., Park, M. H., and Cho, J. (2010). A critical size of silicon nano-anodes for lithium rechargeable batteries. *Angew. Chem. Int. Ed. Engl.* 49, 2146–2149. doi:10.1002/anie.200906287

León, V., Quintana, M., Herrero, M. A., Fierro, J. L., de la Hoz, A., Prato, M., et al. (2011). Few-layer graphenes from ball-milling of graphite with melamine. *Chem. Commun. (Camb.)* 47, 10936–10938. doi:10.1039/c1cc14595a

Li, B., Qi, R., Zai, J., Du, F., Xue, C., Jin, Y., et al. (2016). Silica wastes to high-performance lithium storage materials: a rational designed Al_2O_3 coating assisted magnesiothermic process. *Small* 12, 5281–5287. doi:10.1002/smll.201601914

Li, B., Xiao, Z., Zai, J., Chen, M., Wang, H., Liu, X., et al. (2017). A candidate strategy to achieve high initial coulombic efficiency and long cycle life of Si anode materials: exterior carbon coating on porous Si microparticles. *Mater. Today Energy* 5, 299–305. doi:10.1016/j.mtener.2017.07.006

Li, H., Wang, Z., Chen, L., and Huang, X. (2009). Research on advanced materials for Li-ion batteries. *Adv. Mater. Weinheim* 21, 4593–4607. doi:10.1002/adma.200901710

Liu, J., Kopold, P., Van Aken, P. A., Maier, J., and Yu, Y. (2015). Energy storage materials from nature through nanotechnology: a sustainable route from reed plants to a silicon anode for lithium-ion batteries. *Angew. Chem. Int. Ed. Engl.* 54, 9632. doi:10.1002/anie.201503150

Liu, X. H., Zhang, L. Q., Zhong, L., Liu, Y., Zheng, H., Wang, J. W., et al. (2011). Ultrafast electrochemical lithiation of individual Si nanowire anodes. *Nano Lett.* 11, 2251. doi:10.1021/nl200412p

Liwei, S., Zhen, Z., and Manman, R. (2010). Core double-shell Si@SiO2@C nanocomposites as anode materials for Li-ion batteries. *Chem. Commun.* 46, 2590–2592. doi:10.1039/b925696b

Luo, W., Wang, Y., Chou, S., Xu, Y., Li, W., Kong, B., et al. (2016a). Critical thickness of phenolic resin-based carbon interfacial layer for improving long cycling stability of silicon nanoparticle anodes. *Nano Energy* 27, 255–264. doi:10.1016/j.nanoen.2016.07.006

Luo, W., Wang, Y., Wang, L., Jiang, W., Chou, S. L., Dou, S. X., et al. (2016b). Silicon/mesoporous carbon/crystalline TiO_2 nanoparticles for highly stable lithium storage. *ACS Nano* 10, 10524. doi:10.1021/acsnano.6b06517

Netz, A., and Huggins, R. A. (2004). Amorphous silicon formed in situ as negative electrode reactant in lithium cells. *Solid State Ionics.* 175, 215–219. doi:10.1016/j.ssi.2003.11.048

Ng, S. H., Wang, J., Wexler, D., Konstantinov, K., Guo, Z. P., and Liu, H. K. (2006). Highly reversible lithium storage in spheroidal carbon-coated silicon nanocomposites as anodes for lithium-ion batteries. *Angew. Chem. Int. Ed. Engl.* 45, 6896–6899. doi:10.1002/anie.200601676

Peng, G., Rui, C., Zhou, Y., and Shao, Z. (2010). Si/C composite lithium-ion battery anodes synthesized from coarse silicon and citric acid through combined ball milling and thermal pyrolysis. *Electrochim. Acta* 55, 3876–3883. doi:10.1016/j.electacta.2010.02.006

Rahman, M. A., Song, G., Bhatt, A. I., Wong, Y. C., and Wen, C. (2016). Nanostructured silicon anodes for high-performance lithium-ion batteries. *Adv. Funct. Mater.* 26, 647–678. doi:10.1002/adfm.201502959

Shin, H. C., Corno, J. A., Gole, J. L., and Liu, M. (2005). Porous silicon negative electrodes for rechargeable lithium batteries. *J. Power Sources* 139, 314–320. doi:10.1016/j.jpowsour.2004.06.073

Szczech, J. R., and Jin, S. (2010). Nanostructured silicon for high capacity lithium battery anodes. *Energy Environ. Sci.* 4, 56–72. doi:10.1039/C0EE00281J

Tang, L., Wang, Y., Li, Y., Feng, H., Lu, J., and Li, J. (2009). Preparation, structure, and electrochemical properties of reduced graphene sheet films. *Adv. Funct. Mater.* 19, 2782–2789. doi:10.1002/adfm.200900377

Tao, H. C., Fan, L. Z., Mei, Y., and Qu, X. (2011). Self-supporting Si/reduced graphene oxide nanocomposite films as anode for lithium ion batteries. *Electrochem. Commun.* 13, 1332–1335. doi:10.1016/j.elecom.2011.08.001

Tarascon, J. M., and Armand, M. (2001). Issues and challenges facing rechargeable lithium batteries. *Nature* 414, 359. doi:10.1038/35104644

Teki, R., Datta, M. K., Krishnan, R., Parker, T. C., Lu, T. M., Kumta, P. N., et al. (2009). Nanostructured silicon anodes for lithium ion rechargeable batteries. *Small* 5, 2236–2242. doi:10.1002/smll.200900382

Wang, G., Shen, X., Yao, J., and Park, J. (2009). Graphene nanosheets for enhanced lithium storage in lithium ion batteries. *Carbon N. Y.* 47, 2049–2053. doi:10.1016/j.carbon.2009.03.053

Wang, W., Favors, Z., Ionescu, R., Ye, R., Bay, H. H., Ozkan, M., et al. (2015). Monodisperse porous silicon spheres as anode materials for lithium ion batteries. *Sci. Rep.* 5, 8781. doi:10.1038/srep08781

Winter, M., Besenhard, J. O., Spahr, M. E., and Novák, P. (2010). Insertion electrode materials for rechargeable lithium batteries. *Adv. Mater. Weinheim* 10, 725–763. doi:10.1002/(SICI)1521-4095(199807)10:10<725::AID-ADMA725>3.0.CO;2-Z

Xiang, H., Zhang, K., Ji, G., Lee, J. Y., Zou, C., Chen, X., et al. (2011). Graphene/nanosized silicon composites for lithium battery anodes with improved cycling stability. *Carbon N. Y.* 49, 1787–1796. doi:10.1016/j.carbon.2011.01.002

Xin, X., Zhou, X., Wang, F., Yao, X., Xu, X., Zhu, Y., et al. (2012). A 3D porous architecture of Si/graphene nanocomposite as high-performance anode materials for Li-ion batteries. *J. Mater. Chem.* 22, 7724–7730. doi:10.1039/c2jm00120a

Yan, L., Lin, M., Zeng, C., Chen, Z., Zhang, S., Zhao, X., et al. (2012). Electroactive and biocompatible hydroxyl-functionalized graphene by ball milling. *J. Mater. Chem.* 520, 8367–8371. doi:10.1039/c2jm30961k

Yang, J., Wang, Y., Wei, L., Wang, L., Fan, Y., Wan, J., et al. (2017). Amorphous TiO_2 shells: a vital elastic buffering layer on silicon nanoparticles for high-performance and safe lithium storage. *Adv. Mater.* 29, 1700523. doi:10.1002/adma.201700523

Yi, R., Dai, F., Gordin, M. L., Chen, S., and Wang, D. (2013). Lithium-ion batteries: micro-sized Si-C composite with interconnected nanoscale building blocks as high-performance anodes for practical application in lithium-ion batteries. *Adv. Energy Mater.* 3, 273–273. doi:10.1002/aenm.201370011

Yue, L., Zhong, H., Tang, D., and Zhang, L. (2013). Porous Si coated with S-doped carbon as anode material for lithium ion batteries. *J. Sol. St. Electrochem.* 17, 961–968. doi:10.1007/s10008-012-1944-8

Zhang, S., Du, Z., Lin, R., Jiang, T., Liu, G., Wu, X., et al. (2010). Nickel nanocone-array supported silicon anode for high-performance lithium-ion batteries. *Adv. Mater. Weinheim* 22, 5378–5382. doi:10.1002/adma.201003017

Zhao, W., Fang, M., Wu, F., Wu, H., Wang, L., and Chen, G. (2010a). Preparation of graphene by exfoliation of graphite using wet ball milling. *J. Mater. Chem.* 20, 5817. doi:10.1039/c0jm01354d

Zhao, X., Zhang, Q., Chen, D., and Lu, P. (2010b). Enhanced mechanical properties of graphene-based poly(vinyl alcohol) composites. *Macromolecules* 43, 2357–2363. doi:10.1021/ma902862u

Zheng, Y., Yang, J., Wang, J., and Nuli, Y. (2007). Nano-porous Si/C composites for anode material of lithium-ion batteries. *Electrochim. Acta* 52, 5863–5867. doi:10.1016/j.electacta.2007.03.013

Conflict of Interest Statement: The authors declare that the research was conducted in the absence of any commercial or financial relationships that could be construed as a potential conflict of interest.